Standard and inverse bond percolation of straight rigid rods on square lattices

L. S. Ramirez, P. M. Centres, and A. J. Ramirez-Pastor[*]

Departamento de Física, Instituto de Física Aplicada, Universidad Nacional de San Luis-CONICET,
Ejército de los Andes 950, D5700HHW, San Luis, Argentina

Numerical simulations and finite-size scaling analysis have been carried out to study standard and inverse bond percolation of straight rigid rods on square lattices. In the case of standard percolation, the lattice is initially empty. Then, linear bond k-mers (sets of k linear nearest-neighbor bonds) are randomly and sequentially deposited on the lattice. Jamming coverage $p_{j,k}$ and percolation threshold $p_{c,k}$ are determined for a wide range of k ($1 \leqslant k \leqslant 120$). $p_{j,k}$ and $p_{c,k}$ exhibit a decreasing behavior with increasing k, $p_{j,k \to \infty} = 0.7476(1)$ and $p_{c,k \to \infty} = 0.0033(9)$ being the limit values for large k-mer sizes. $p_{j,k}$ is always greater than $p_{c,k}$, and consequently, the percolation phase transition occurs for all values of k. In the case of inverse percolation, the process starts with an initial configuration where all lattice bonds are occupied and, given that periodic boundary conditions are used, the opposite sides of the lattice are connected by nearest-neighbor occupied bonds. Then, the system is diluted by randomly removing linear bond k-mers from the lattice. The central idea here is based on finding the maximum concentration of occupied bonds (minimum concentration of empty bonds) for which connectivity disappears. This particular value of concentration is called the inverse percolation threshold $p_{c,k}^i$, and determines a geometrical phase transition in the system. On the other hand, the inverse jamming coverage $p_{j,k}^i$ is the coverage of the limit state, in which no more objects can be removed from the lattice due to the absence of linear clusters of nearest-neighbor bonds of appropriate size. It is easy to understand that $p_{j,k}^i = 1 - p_{j,k}$. The obtained results for $p_{c,k}^i$ show that the inverse percolation threshold is a decreasing function of k in the range $1 \leqslant k \leqslant 18$. For $k > 18$, all jammed configurations are percolating states, and consequently, there is no nonpercolating phase. In other words, the lattice remains connected even when the highest allowed concentration of removed bonds $p_{j,k}^i$ is reached. In terms of network attacks, this striking behavior indicates that random attacks on single nodes ($k = 1$) are much more effective than correlated attacks on groups of close nodes (large k's). Finally, the accurate determination of critical exponents reveals that standard and inverse bond percolation models on square lattices belong to the same universality class as the random percolation, regardless of the size k considered.

I. INTRODUCTION

Percolation is currently a very active field of research in statistical mechanics and has been attracting a great deal of interest for a long time [1–4]. This is due in part to the fact that this system is known to provide a useful model for studies of second-order phase transitions.

In the standard lattice percolation model, a single site (or a bond connecting two sites) is occupied with probability p. For a precise value of p, a cluster of nearest-neighbor sites (bonds) extends from one side to the opposite one of the system. This particular value of concentration rate is named percolation threshold p_c, and determines a second-order phase transition in the system, which is characterized by well-defined critical exponents [2]. More general percolation problems can be formulated by including deposition of elements occupying more than one site (k-mers). Thus, percolation of k-mers on different lattices in plane and multidimensional space has been intensively studied [5–15].

Percolation theory can also be used to describe the response of a network to the removal of sites or bonds, the phenomena of primary interest in robustness [16,17]. The mathematical

model of such a process can be thought of as an inverse percolation problem [18]. Most developments in inverse percolation have mainly dealt with the removal of singly nodes, much less attention has been given to the removal of clusters of nodes. In this line, two previous articles [19,20] referred to as papers I and II, respectively, were devoted to the study of inverse site percolation by removing straight rigid rods from two-dimensional (2D) lattices.

In paper I, square surfaces were used. The process started with an initial configuration, where all lattice sites were occupied and, obviously, the opposite sides of the lattice were connected by nearest-neighbor occupied sites. Then, the system was diluted by randomly removing linear clusters of k consecutive sites (k-mers) from the surface. The central idea of paper I was based on finding the maximum concentration of occupied sites for which connectivity disappears. This particular value of concentration was called the inverse percolation threshold. A similar study for triangular lattices was carried out in paper II. The results obtained in both papers indicate that, from a certain value of k ($k = 7$ for square lattices and $k = 11$ for triangular lattices), the inverse percolation threshold is a decreasing function with the k-mer size.

The problem of inverse percolation offers a simplified representation of an irreversible reaction-annihilation process

[*]antorami@unsl.edu.ar

[21,22]. In fact, we can think of a set of k nearest-neighbor particles which react and desorb from the surface, leaving behind k holes. As mentioned above, the inverse percolation model can be also used to study robustness in networks. From this point of view, we can think of a regular lattice as a network whose nodes (sites or bonds) are occupied. Then, a fraction of elements (sites or bonds) is removed, with the aim of finding out how their absence impacts the integrity of the lattice. If this fraction is small, the few missing nodes do little damage to the network. As the fraction of removed elements is increased above a certain critical value, the initial large cluster breaks into tiny noncommunicating components and connectivity between both sides of the lattice disappears.

The study of robustness as an inverse percolation problem is important for many fields [18]. In communications and information theory, it can be used to find out what fraction of nodes must break down so that a network turns into isolated clusters that are unable to communicate with each other [23,24]. Recently, the vulnerability of networks during the process of cascading failures has received great attention in the literature [25,26]. In Refs. [25,26], the authors studied the influence of the characteristics of the initial attack on the vulnerability of the networks. The obtained results revealed that random attacks on single nodes are much more effective than correlated attacks on groups of close nodes.

The results in Refs. [25,26] are consistent with those from papers I and II, where it was shown that the inverse percolation threshold decreases as the k-mer size increases ($k \geqslant 7$ for square lattices and $k \geqslant 11$ for triangular lattices). In other words, papers I and II indicate that, for a same fraction of removed sites (or attack, in the terminology of Refs. [25,26]), the robustness of the network increases with the attack size (k). These findings encourage us to continue our research on inverse percolation as a simple model to study the robustness (or vulnerability) of a network against failure of either nodes or links.

As discussed in previous paragraphs, papers I and II treated the problem of inverse percolation on a lattice of sites. This situation has permitted us to extract general conclusions about the connectivity properties of states generated by removing linear clusters of sites from 2D lattices. The same has not happened in the case of a lattice of bonds, where the problem of inverse percolation has not yet been addressed. The objective of this paper is to provide a thorough study in this direction. For this purpose, extensive numerical simulations, supplemented by analysis using finite-size scaling theory, have been carried out to study the problem of inverse percolation by removing clusters of bonds from lattices with square geometry. The standard percolation problem of linear bond k-mers was also revisited and extended to longer objects: $1 \leqslant k \leqslant 120$. In addition, the critical exponents for standard and inverse problems are reported for the first time in the literature.

The paper is organized as it follows. In Sec. II, standard percolation of linear bond k-mers is studied. The problem of inverse percolation by removing linear bond k-mers from square lattices is addressed in Sec. III. The analysis of the critical exponents obtained by using finite-size scaling theory is discussed in Sec. IV. Finally, the conclusions are drawn in Sec. V.
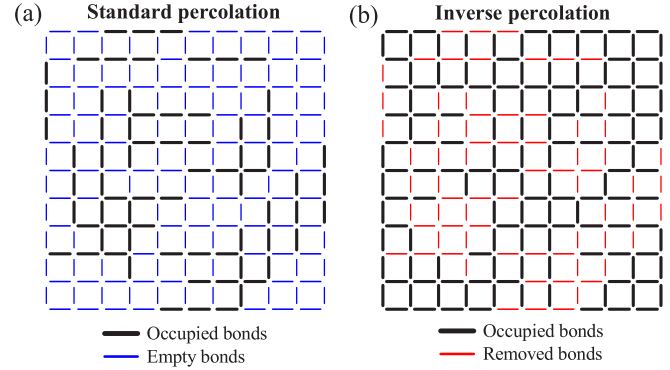

FIG. 1. (a) Schematic representation of a square lattice, initially empty, in which some linear bond 3-mers have been deposited. Thick (black) lines and thin (blue) lines represent 3-mer units (occupied bonds) and empty (nonoccupied) bonds, respectively. (b) Schematic representation of an initially fully occupied square lattice in which some linear bond 3-mers have been removed. Thick (black) lines and thin (red) lines represent occupied and removed bonds, respectively.

II. STANDARD PERCOLATION OF LINEAR BOND K-MERS ON SQUARE LATTICES

We consider a periodic square lattice of linear size L (L-lattice) on which straight rigid rods [or linear bond k-mers, see Fig. 1(a)] are deposited at random. The procedure is as follows. A set of k linear nearest-neighbor bonds (aligned along one of two lattice axes) is randomly chosen; if it is vacant, the bond k-mer is then deposited onto the lattice. Otherwise, the attempt is rejected. In any case, the procedure is iterated until N bond k-mers are deposited and the desired concentration $p = kN/2L^2$ is reached.

Figure 1(a) schematically illustrates the system described in the paragraph above. A typical configuration of linear bond 3-mers is shown. Thick (black) lines and thin (blue) lines represent 3-mer units (occupied bonds) and empty (nonoccupied) bonds, respectively.

Due to the blocking of the lattice by the already randomly deposited elements, the limiting or "jamming coverage," $p_j = p(t = \infty)$, is less than that corresponding to the close packing ($p_j < 1$) [27]. Note that $p(t)$ represents the total fraction of bonds occupied at time t by the deposited objects. Consequently, p ranges from 0 to p_j for objects occupying more than one bond.

To calculate the jamming limits for different values of k, we use the probability $W_L(p)$ that a lattice composed of $L \times L$ elements reaches a coverage p [28]. In the simulations, the procedure to determine $W_L(p)$ consists of the following steps: (a) the construction of the $L \times L$ lattice (initially empty) and (b) the deposition of bonds on the lattice up to the jamming limit p_j. In the late step, the quantity $m_i(p)$ is calculated as

$$m_i(p) = \begin{cases} 1 & \text{for } p \leqslant p_j \\ 0 & \text{for } p > p_j. \end{cases} \tag{1}$$

n runs of such two steps (a)-(b) are carried out for obtaining the number $m(p)$ of them for which a lattice reaches a bond
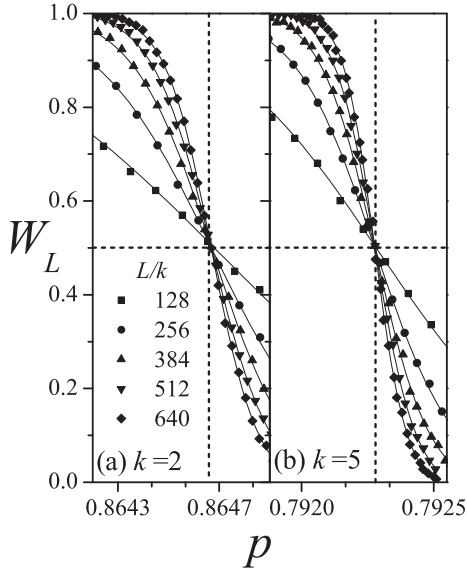
FIG. 2. Curves of the jamming probability W_L as a function of the fraction of occupied bonds p for two values of k-mer size ($k = 2$, curves on the left, and $k = 5$, curves on the right) and lattice sizes ranging between $L/k = 128$ and $L/k = 640$. The statistical error is smaller than the symbol size. Horizontal dashed line shows the W_L^* point. Vertical dashed lines denote the jamming thresholds in the thermodynamic limit.

coverage p,

$$m(p) = \sum_{i=1}^{n} m_i(p). \qquad (2)$$

Then, $W_L(p) = m(p)/n$ is defined and the procedure is repeated for different values of L. A set of $n = 10^5$ independent samples is numerically prepared for several values of the lattice size ($L/k = 128, 256, 384, 512, 640$). The L/k ratio is kept constant to prevent spurious effects due to the size k in comparison with the lattice linear size L.

As shown in previous papers [28–30], the jamming coverage can be estimated from the curves of the probabilities W_L plotted versus p for several lattice sizes. In the vicinity of the limit coverage, the probabilities show a strong dependence on the system size. However, at the jamming point, the probabilities adopt a nontrivial value W_L^*, irrespective of system sizes in the scaling limit. Thus, plotting $W_L(p)$ for different linear dimensions L yields an intersection point W_L^*, which gives an accurate estimation of the jamming coverage in the infinite system.

In Fig. 2, the probabilities $W_L(p)$ are shown for different values of L/k (as indicated) and two typical cases: $k = 2$ (left); and $k = 5$ (right). From the inspection of Fig. 2 (and from data do not shown here for a sake of clarity), it can be seen that: (a) for each k, the curves cross each other in a unique point W_L^*; (b) those points do not modify their numerical value for the different cases studied, being $W_L^* \approx 0.5$; and (c) those points are located at very well-defined values in the p axes determining the jamming threshold for each k, $p_{j,k}$. In the case of Fig. 2, $p_{j,k=2} = 0.86467(4)$ and $p_{j,k=5} = 0.79228(3)$.

The procedure of Fig. 3 was repeated for k between 2 and 120 (the case $k = 1$ is trivial, $p_{j,k=1} = 1$). The curves
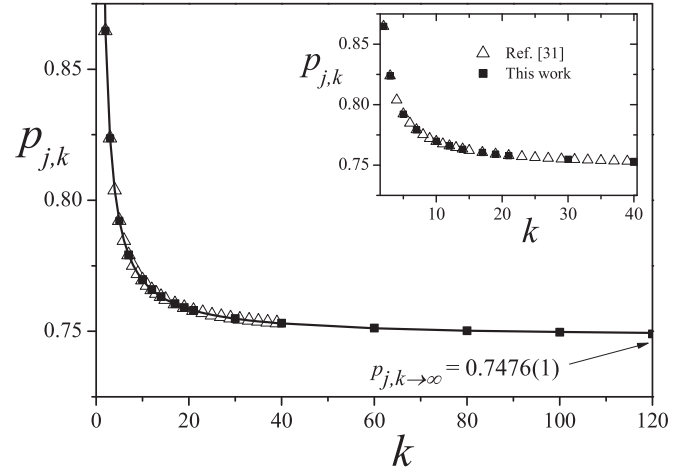

FIG. 3. Jamming coverage $p_{j,k}$ as a function of k for linear bond k-mers on square lattices with k between 2 and 120. Inset: As main figure for $2 \leqslant k \leqslant 40$. Solid squares represent simulation results obtained in this work (the error in each measurement is smaller than the size of the symbols), open triangles denote data from the literature [31], and the solid line corresponds to the fitting function as discussed in the text.

corresponding to $k = 80$, $k = 100$, and $k = 120$ were calculated for $L/k = 60$ and $L/k = 80$, with an effort reaching almost the limits of our computational capabilities. The results are shown in Fig. 3. In the range $2 \leqslant k \leqslant 40$, the values obtained of $p_{j,k}$ coincide, within the statistical errors, with those reported in Ref. [31] (see inset of Fig. 3). These results validate our program and calculation method.

For large values of k, the data follow a similar behavior to that predicted by Bonnier et al. [9] for linear site k-mers on square lattices, and Perino et al. for linear site k-mers on triangular lattices [30]: $p_{j,k} = A_j + B_j/k + C_j/k^2$ ($k \geqslant 1$), being $A_j = p_{j,k \to \infty} = 0.7476(1)$ the result for the limit coverage of a square lattice by infinitely long bond k-mers. In addition, $B_j = 0.2165(5)$ and $C_j = 0.0360(5)$. The value $p_{j,k \to \infty} = 0.7476(1)$ improves the previously obtained in Ref. [31], showing the advantages of having reached larger sizes for the objects.

Once the limiting parameters $p_{j,k}$ are determined, the next step is to calculate the percolation threshold $p_{c,k}$. For this purpose, the probability $R_{L,k}^X(p)$ that a lattice composed of $2L^2$ bonds percolates at the concentration p of occupied bonds can be defined [2]. The subindex k indicates that the density p was reached by depositing linear bond k-mers. Here, the following definitions can be given according to the meaning of X [32]:

(1) $R_{L,k}^R(p)$: the probability of finding a rightward percolating cluster, along the x direction,

(2) $R_{L,k}^D(p)$: the probability of finding a downward percolating cluster, along the y direction.

Other useful definitions for the finite-size analysis are:

(3) $R_{L,k}^U(p)$: the probability of finding a cluster which percolates on any direction,

(4) $R_{L,k}^I(p)$: the probability of finding a cluster which percolates in the two (mutually perpendicular) directions,

(5) $R_{L,k}^A(p) = \frac{1}{2}[R_{L,k}^U(p) + R_{L,k}^I(p)]$.

Numerical simulations have been developed to determine each of the previously mentioned quantities. Each simulation run consists of the following two steps: (a) the construction of the square lattice for the desired fraction p of bonds; and (b) the cluster analysis by using the Hoshen and Kopelman algorithm [33]. In the last step, the size of the largest cluster S_L is determined, as well as the existence of a percolating island. A total of m_L independent runs of such two steps procedure were carried out for each lattice size L. From these runs a number m_L^X of them present a percolating cluster, this is done for the desired criterion among $X = \{R, D, I, U, A\}$. Then, $R_{L,k}^X(p) = m_L^X/m_L$ is defined and the procedure is repeated for different values of L, p, and k-mer size.

Besides the different probabilities $R_{L,k}^X(p)$, the percolation order parameter ($P = \langle S_L \rangle / M$) [34,35] was measured, where S_L represents the size of the largest cluster and $\langle ... \rangle$ means an average over simulation runs.

The quantities related with the order parameter, such as the susceptibility χ and the reduced fourth-order cumulant U_L introduced by Binder [36], were calculated as

$$\chi = [\langle S_L^2 \rangle - \langle S_L \rangle^2]/M, \tag{3}$$

and

$$U_L = 1 - \frac{\langle S_L^4 \rangle}{3 \langle S_L^2 \rangle^2}. \tag{4}$$

In our percolation simulations, we used $m_L = 10^5$ independent random samples. In addition, for each value of k and p, the effect of finite size was investigated by examining square lattices with $L/k = 128, 256, 384, 512, 640$. As can be appreciated, this represents extensive calculations from the computational point of view. From this, finite-scaling theory can be used to determine the percolation threshold and the critical exponents with reasonable accuracy.

The standard theory of finite-size scaling [2,32,36] allows for various efficient routes to estimate the percolation threshold from simulation data. One of these methods, which will be used in what follows, is from the maxima of the curves of $R_{L,k}^X(p)$.

In order to express these curves as a function of continuous values of p, it is convenient to fit $R_{L,k}^X(p)$ with some approximating function through the least-squares method. The fitting curve is the *error function* because $dR_{L,k}^X(p)/dp$ is expected to behave like the Gaussian distribution [32,37,38],

$$\frac{dR_{L,k}^X}{dp} = \frac{1}{\sqrt{2\pi}\Delta_{L,k}^X} \exp\left\{-\frac{1}{2}\left[\frac{p - p_{c,k}^X(L)}{\Delta_{L,k}^X}\right]^2\right\}, \tag{5}$$

where $p_{c,k}^X(L)$ is the concentration at which the slope of $R_{L,k}^X(p)$ is the largest and $\Delta_{L,k}^X$ is the standard deviation from $p_{c,k}^X(L)$.

Once obtained the values of $p_{c,k}^X(L)$ for different lattice sizes, a scaling analysis can be done [2]. Thus, we have

$$p_{c,k}^X(L) = p_{c,k}^X(\infty) + A^X L^{-1/\nu}, \tag{6}$$

where A^X is a nonuniversal constant and ν is the critical exponent of the correlation length which will be taken as 4/3 for the present analysis, since, as it will be shown below, our model belongs to the same universality class as random percolation [2].
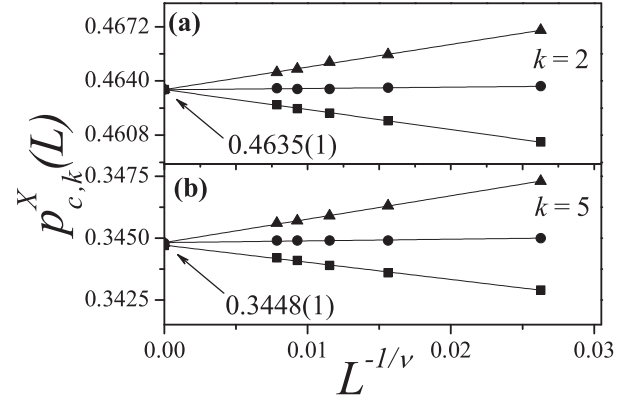

FIG. 4. Extrapolation of the percolation threshold for an L-lattice $p_{c,k}^X(L)$ ($X = \{I, U, A\}$) toward the thermodynamic limit according to the theoretical prediction given by Eq. (6). Triangles, circles, and squares denote the values of $p_{c,k}^X(L)$ obtained by using the criteria I, A, and U, respectively. Two values of k are presented: (a) $k = 2$ and (b) $k = 5$. The bar error in each measurement is smaller than the size of the symbols.

Figure 4 shows the plots toward the thermodynamic limit of $p_{c,k}^X(L)$ according to Eq. (6) for (a) $k = 2$ and (b) $k = 5$. From extrapolations it is possible to obtain $p_{c,k}^X(\infty)$ for the criteria I, A, and U. Combining the three estimates for each case, the final values of $p_{c,k}(\infty)$ can be obtained. Additionally, the maximum of the differences between $|p_{c,k}^U(\infty) - p_{c,k}^A(\infty)|$ and $|p_{c,k}^I(\infty) - p_{c,k}^A(\infty)|$ gives the error bar for each determination of $p_{c,k}(\infty)$. In this case, the values obtained were: $p_{c,k=2}(\infty) = 0.4635(1)$ and $p_{c,k=5}(\infty) = 0.3448(1)$. For the rest of the paper, we will denote the percolation threshold for each size k by $p_{c,k}$ [for simplicity we will drop the "(∞)"].

The procedure of Fig. 4 was repeated for k ranging between 2 and 120 (as it is well-known, $p_{c,k=1} = 0.5$ [2]). The points corresponding to $k = 50$, $k = 60$, and $k = 80$ were calculated for $L/k = 128$ and $L/k = 256$. In the case of $k = 100$ and $k = 120$, two relatively small values of L/k were used ($L/k = 64$ and $L/k = 128$), with an effort reaching almost the limits of our computational capabilities. The results are shown in Fig. 5 (solid squares).

At the beginning, for small values of k, the curve rapidly decreases. However, it flattens out for larger values of k and finally asymptotically converges toward a definite value as $k \to \infty$. Figure 5 also includes the values of the percolation threshold reported in Ref. [31] (open triangles). As it can be observed, our results are consistent with the previous ones obtained by M. Dolz *et al.* [31].

For all the range of studied sizes, the percolation threshold decreases upon increasing k. This result contrasts with the behavior obtained for site percolation of straight rigid rods on square [13] and triangular [30] lattices. In Refs. [13,30], a nonmonotonic k-mer size dependence was reported for the percolation threshold. Namely, the percolation threshold decreases for small particle sizes, goes through a minimum at $k \approx 12$–13, and finally increases as k increases. The nonmonotonic behavior has been explained accounting for the local alignment effects occurring for large values of k. In the case of bond percolation of linear bond k-mers on square lattices, these
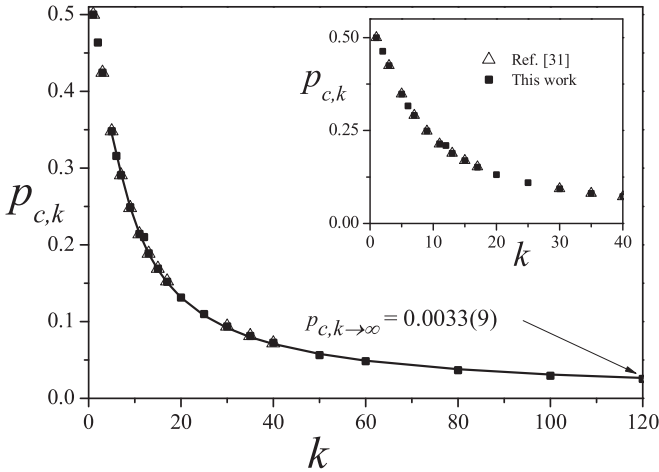
FIG. 5. Percolation threshold $p_{c,k}$ as a function of k for linear bond k-mers on square lattices (solid squares). The behavior of the fitting curve is described according to Eq. (7). The asymptotic limit $p_{c,k\to\infty} = 0.0033(9)$ is shown. The size of the points is larger than the corresponding error bars. Open triangles denote previous data in the literature [31].

effects are not detected in the range of values of k between 1 and 120.

Following a similar scheme to that proposed in Fig. 3, the curve of $p_{c,k}$ versus k was fitted to a function

$$p_{c,k} = A_c + \frac{B_c}{k} + \frac{C_c}{k^2} \quad (k \geqslant 5), \qquad (7)$$

$A_c = p_{c,k\to\infty} = 0.0033(9)$ being the limit percolation threshold by infinitely long bond k-mers on square lattices, $B_c = 2.84(3)$ and $C_c = -5.7(2)$.

The value of $p_{c,k\to\infty} = 0.0033(9)$ obtained in Fig. 5 corrects the previously reported value of $p_{c,k\to\infty} = 0.071(1)$ [31]. Due to the values of L and k studied in this contribution, our estimate of $p_{c,k\to\infty}$ is expected to be more accurate than that reported previously.

III. INVERSE PERCOLATION BY REMOVING LINEAR BOND K-MERS FROM SQUARE LATTICES

As mentioned in Sec. I, percolation theory can also be used to describe the response of a network to the removal of sites or bonds. The process, known as inverse percolation [19,20], starts with a fully occupied lattice. Then, the system is diluted by randomly removing elements (sites or bonds) from the surface. The central idea of the inverse percolation model is based on finding the minimum concentration of elements for which connectivity disappears. The problem results quite simple for the case of removing single sites or bonds, when the inverse and standard problems are symmetrical. However, if some sort of correlation exists, as in the case of removing clusters of lattice elements, the statistical problem becomes exceedingly difficult, and the percolation threshold has to be estimated numerically by means of computer simulations.

In the present paper, we consider a periodic square lattice of linear size L where, initially, every bond is occupied. Then, the system is diluted by removing bond k-mers according to the following procedure: (i) a set of k linear nearest-neighbor

bonds (aligned along one of the lattice axes) is randomly chosen; (ii) if the selected bonds are occupied, the bond k-mer is removed from the lattice. Otherwise, the attempt is rejected. When N bond k-mers are removed, the concentration of absent and present bonds is $p^* = kN/2L^2$ and $p = (2L^2 - kN)/2L^2$ ($p = 1 - p^*$), respectively.

The first step to calculate the inverse percolation properties of the system is to determine the space of allowed p values ($p^i_{j,k} \leqslant p \leqslant 1$). $p^i_{j,k}$ is the coverage of the limit state, in which no more objects can be removed from the lattice due to the absence of linear clusters of nearest-neighbor bonds of appropriate size. It is easy to understand that $p^i_{j,k} = 1 - p_{j,k}$, where $p_{j,k}$ represents the jamming coverage in Eq. (7). Thus,

$$p^i_{j,k} = 1 - p_{j,k} = 0.2524 - \frac{0.2165}{k} - \frac{0.0360}{k^2} \quad (k \geqslant 1). \qquad (8)$$

Interested readers are referred to paper I for a more complete description of Eq. (8).

Once the jamming limit is determined, the inverse percolation threshold $p^i_{c,k}$ can be calculated. As in previous section, $p^i_{c,k}$ is obtained from the probabilities $R^X_{L,k}(p)$ ($X = \{R,D,I,U,A\}$). In this case, the subindex k indicates that the density p was reached by removing sets of k bonds (bond k-mers). Each simulation run consists of the following two steps: (a) the construction of the lattice for the desired fraction p of occupied bonds. For this purpose, a fraction of $p^* = 1 - p$ bonds are removed according to the procedure described above, and (b) the cluster analysis using the Hoshen and Kopelman algorithm [33]. As in the case of standard percolation (Sec. II), we used $m_L = 10^5$ independent random samples. In addition, for each value of k and p, the effect of finite size was investigated by examining square lattices with $L/k = 128, 256, 384, 512, 640$.

The inverse percolation threshold can be obtained from the extrapolation toward the thermodynamic limit of $p^{i,X}_{c,k}(L)$ ($X = \{R,D,I,U,A\}$) according to Eq. (6). This procedure is illustrated in Fig. 6 for $k = 2$ and $k = 5$. Combining the three estimates for each case, the final values of $p^i_{c,k}(\infty)$ is obtained. In this case, $p^i_{c,k=2} = 0.4499(2)$ and $p^i_{c,k=5} = 0.3668(1)$. As in the previous section, we will drop the "(∞)."

The study in Fig. 6 was repeated for k in the range 2–120. The results are shown in Fig. 7 (open circles). Figure 7 also includes $p^i_{j,k}$ as a function of k [Eq. (8), solid circles]. The region above the curve of $p^i_{j,k}$ represents the space of all the allowed values of p (values of p which can be reached by removing straight rigid bond k-mers from the surface). On the other hand, the region below to the curve of $p^i_{j,k}$ corresponds to a forbidden region of the p space.

The inverse percolation threshold is a monotonically decreasing function of k in the interval [1, 18]. The inset in Fig. 7 shows a zoom of the main figure around $k = 18$. For $k > 18$, all jammed configurations are percolating states, and consequently, there is no nonpercolating phase. This phenomenon can be better understood by examining Fig. 8, where the functions $R^X_{L,k}(p)$ ($X = I,U,A$) have been plotted for $k = 17$ (a), $k = 18$ (b), $k = 19$ (c). For clarity, simulation results from only three lattice sizes are shown ($L/k = 64$, squares; $L/k = 128$, circles; and $L/k = 256$, triangles).
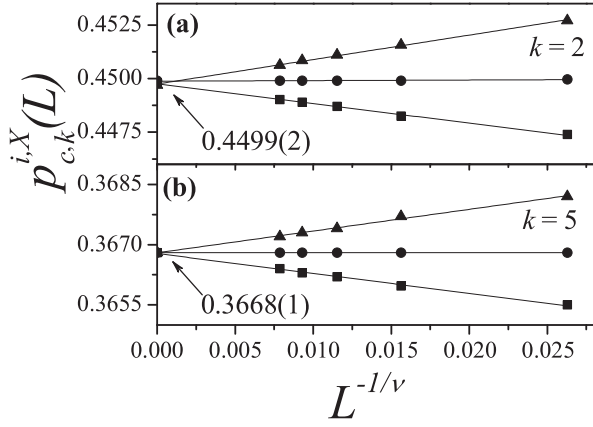
FIG. 6. Extrapolation of the inverse percolation threshold for an L-lattice $p_{c,k}^{i,X}(L)$ ($X = \{I, U, A\}$) toward the thermodynamic limit according to the theoretical prediction given by Eq. (6). Triangles, circles, and squares denote the values of $p_{c,k}^{i,X}(L)$ obtained by using the criteria I, A, and U, respectively. Two values of k are presented: (a) $k = 2$; and (b) $k = 5$. The bar error in each measurement is smaller than the size of the symbols.

In the case of $k = 17$ and $k = 18$, the curves for different lattice sizes cross each other in a unique point, which depends on the criterion X used. Those points are located at very well-defined values in the p axes (see vertical dashed lines) determining the inverse percolation threshold for each k: $p_{c,k=17}^{i} = 0.2469(1)$ and $p_{c,k=18}^{i} = 0.2405(2)$. Vertical solid line in Fig. 8(b) indicates the corresponding jamming coverage, $p_{j,k=18}^{i} = 0.24033(7)$.

The situation is different for $k = 19$, where the curves of $R_{L,k}^{X}(p)$ remain constant and equal to 1 up to the jamming coverage $p_{j,k=19}^{i} = 0.24096(3)$ (vertical solid line in the figure). This finding is a clear indication that (i) the percolation
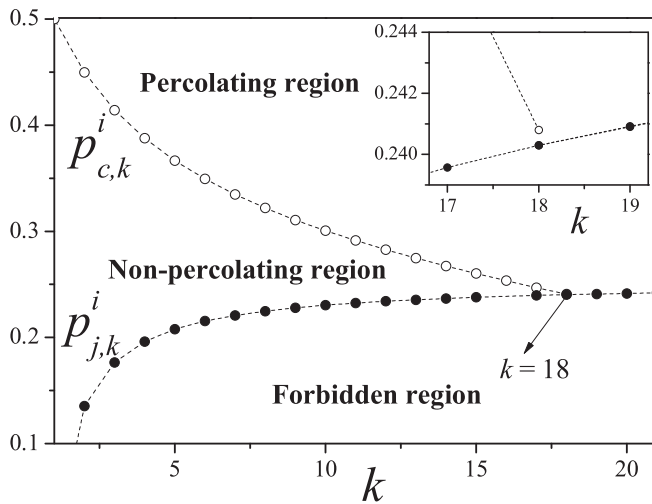

FIG. 7. Inverse percolation threshold $p_{c,k}^{i}$ (open circles) and limit coverage $p_{j,k}$ (solid circles) as a function of k for linear bond k-mers on square lattices. The size of the points is larger than the corresponding error bars. Inset: Zoom of the main figure for $17 \leqslant k \leqslant 19$.
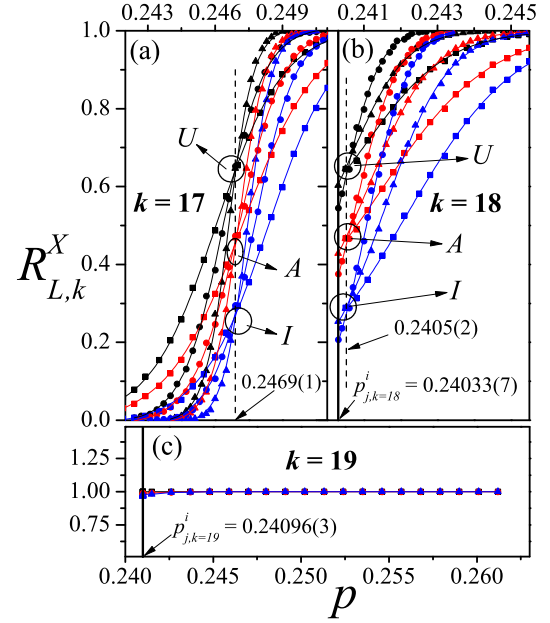

FIG. 8. Fraction of percolating lattices $R_{L,k}^{X}$ [$X = I$ (blue curves), U (red curves), A (black curves)] as a function of the concentration θ for $k = 17$ (a), $k = 18$ (b), and $k = 19$ (c), and three different lattice sizes: $L/k = 64$, squares; $L/k = 128$, circles; and $L/k = 256$, triangles. The statistical error is smaller than the symbol size.

phase transition disappeared, and (ii) there is only one phase (the percolating phase) in the whole range of allowed values of p.

Returning to Fig. 7, the percolation behavior of the system can be summarized as follows: (1) for $1 \leqslant k \leqslant 18$, the curve of $p_{c,k}^{i}$ divides the space of allowed values of p in a percolating region ($p > p_{c,k}^{i}$) and a nonpercolating region ($p_{j,k}^{i} < p < p_{c,k}^{i}$); and (2) for $k > 18$, the entire space of allowed values of p ($p > p_{j,k}^{i}$) is a percolating region.

The interplay between the percolation and the jamming effects is responsible for the existence of a maximum value of k (in this case, $k = 18$) from which the percolation phase transition no longer occurs. This behavior had not been observed previously. In fact, in the case of inverse percolation of linear site k-mers on square and triangular lattices, percolating and nonpercolating phases extend to infinity in the space of the parameter k [19,20].

In terms of vulnerability and network attacks, the decreasing behavior of $p_{c,k}^{i}$ as a function of k indicates that the robustness of the network increases with the attack size (k). As an illustrative example, it is necessary to remove almost 3/4 of the links to disconnect a network by removing sets of 16 linear nearest-neighbor bonds ($p_{c,k=16}^{i} \approx 0.25$). The same effect can be achieved by removing only 1/2 of isolated links ($p_{c,k=1}^{i} = 0.5$). Moreover, for large k-mers ($k > 18$), the lattice remains connected even when the highest allowed concentration of removed bonds $p_{j,k}^{i}$ is reached. These results are consistent with those in Refs. [25,26], where it was shown that random attacks on single nodes are much more effective than correlated attacks on groups of close nodes.
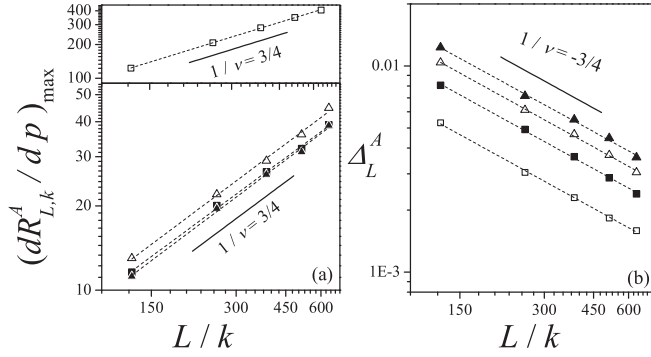
FIG. 9. (a) Maximum of the derivative of the A percolation probability $(dR^A_{L,k}/dp)_{max}$ as a function of L/k (in a log-log scale) for four different cases: standard percolation, $k = 2$ (solid triangles); standard percolation, $k = 5$ (solid squares); inverse percolation, $k = 2$ (open triangles); and inverse percolation, $k = 5$ (open squares). The bar error in each measurement is smaller than the size of the symbols. According to Eq. (9) the slope of each line corresponds to $1/\nu = 3/4$. (b) Natural logarithm of the standard deviation in Eq. (5) $\ln(\Delta^A_{L,k})$ as a function of L/k (in a log-log scale) for the same cases shown in part (a). According to Eq. (10), the slope of each line corresponds to $-1/\nu = -3/4$.

IV. CRITICAL EXPONENTS AND UNIVERSALITY

A complete analysis of the studied phenomena requires establishing the universality class of the phase transition which the system undergoes. This universality is determined by the value of the critical exponents ν, β, and γ. In the case of site percolation of linear k-mers on square lattices, the obtained results for both standard [7] and inverse [19] problems revealed that, in all the cases, the phase transition occurring in the system belongs to the random percolation universality class. Since there is no similar report for the case of bond percolation, the main purpose of this section is to carry out a thorough study of critical exponents in order to determine the universality class of the standard and inverse bond percolation of straight rigid rods on square lattices.

The critical exponent ν can be calculated from the maximum of the function in Eq. (5) [2]:

$$\left(\frac{dR^X_{L,k}}{dp}\right)_{max} \propto L^{1/\nu}. \tag{9}$$

If $(dR^X_{L,k}/dp)_{max}$ is plotted as a function of L/k in log-log scale, the slope of the line will correspond to $1/\nu$.

Figure 9(a) shows $\ln[(dR^A_{L,k}/dp)_{max}]$ as a function of $\ln(L)$ (log-log functional dependence) for four different cases: standard percolation, $k = 2$ (solid triangles); standard percolation, $k = 5$ (solid squares); inverse percolation, $k = 2$ (open triangles); and inverse percolation, $k = 5$ (open squares). The slope of the lines corresponds to $1/\nu$ and, as can be observed, remain constant (and close to 3/4) for all studied cases. Thus, $\nu = 1.33(1)$ for $k = 2$ (standard percolation) and $\nu = 1.35(2)$ for $k = 5$ (standard percolation); $\nu = 1.33(1)$ for $k = 2$ (inverse percolation) and $\nu = 1.34(2)$ for $k = 5$ (inverse percolation).

Another alternative way to obtain ν is from the divergence of the root mean square deviation of the threshold observed

from their average values, $\Delta^X_{L,k}$ [2],

$$\Delta^X_{L,k} \propto L^{-1/\nu}. \tag{10}$$

In this case, the slope of the lines $\Delta^X_{L,k}$ versus L/k (log-log scale) will correspond to $-1/\nu$.

Figure 9(b) shows $\ln(\Delta^A_{L,k})$ as a function of $\ln(L)$ (log-log functional dependence) for the same cases studied in the main figure. According to Eq. (10), the slope of each line corresponds to $-1/\nu$. Again, the slopes of the lines remain constant and close to $-3/4$. Through this method, $\nu = 1.33(1)$ for $k = 2$ (standard percolation) and $\nu = 1.33(3)$ for $k = 5$ (standard percolation); $\nu = 1.33(1)$ for $k = 2$ (inverse percolation) and $\nu = 1.33(1)$ for $k = 5$ (inverse percolation).

The study in Fig. 9 was repeated for different values of k and I, U, and A criteria (not shown here for the sake of space). In all cases, the results obtained for ν coincide, within numerical errors, with the exact value of the critical exponent of the ordinary percolation, namely, $\nu = 4/3$ [2].

Once we know ν, the exponents γ and β can be determined by the analysis of the susceptibility and the percolation order parameter, respectively. According to the finite-size scaling theory [2], the behavior of χ and P at criticality [2] is

$$\chi = L^{\gamma/\nu}\overline{\chi}(u), \tag{11}$$

$$P = L^{-\beta/\nu}\overline{P}(u'), \tag{12}$$

with $u = (p - p_{c,k})L^{1/\nu}$, $u' = |p - p_{c,k}|L^{1/\nu}$, and $\overline{\chi}$ and $\overline{P}$ are the corresponding scaling functions.

At the point that each function is maximal, $u = \text{const.}$,

$$\chi_{max} \propto L^{\gamma/\nu}, \tag{13}$$

$$\left(\frac{dP}{dp}\right)_{max} = L^{(-\beta/\nu+1/\nu)}\overline{P}(u') \propto L^{(1-\beta)/\nu}. \tag{14}$$

When Eqs. (13) and (14) are illustrated in a log-log scale, the slopes of the corresponding lines are γ/ν and $(1 - \beta)/\nu$, respectively. As an illustrative example, the procedure detailed above is shown in Fig. 10 for the same cases studied in Fig. 9. The values obtained in the figure are $\gamma = 2.40(1)$ and $\beta = 0.143(8)$ for $k = 2$ (standard percolation); $\gamma = 2.40(2)$ and $\beta = 0.144(7)$ for $k = 5$ (standard percolation); $\gamma = 2.40(3)$ and $\beta = 0.144(9)$ for $k = 2$ (inverse percolation); and $\gamma = 2.39(1)$ and $\beta = 0.144(8)$ for $k = 5$ (inverse percolation). Simulation data are consistent with the exact values of the critical exponents of the ordinary percolation, $\gamma = 43/18$ and $\beta = 5/36$.

The protocol described in Figs. 9 and 10 was repeated for values of k between 2 and 120 (these data are not shown here for brevity). In all cases, the values obtained for ν [Fig. 9], γ [Fig. 10(a)], and β [Fig. 10(b)] clearly indicate that, for finite values of k, the problems of standard and inverse bond percolation on square lattices belong to the same universality class as the random percolation, regardless of the size k considered.
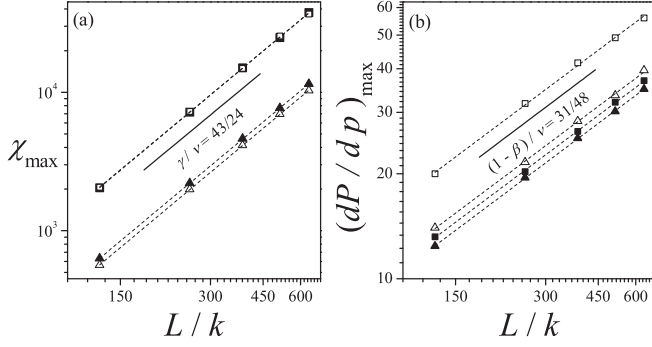
FIG. 10. (a) Maximum of the susceptibility $\chi_{\max}$ as a function of L/k (in a log-log scale) for the following cases: standard percolation, $k = 2$ (solid triangles); standard percolation, $k = 5$ (solid squares); inverse percolation, $k = 2$ (open triangles); and inverse percolation, $k = 5$ (open squares). The bar error in each measurement is smaller than the size of the symbols. The slope of each line corresponds to $\gamma/\nu = 43/24$. (b) Maximum of the derivative of the percolation order parameter $(dP/dp)_{\max}$ as a function of L/k (in a log-log scale) for the same cases reported in part (a). According to Eq. (14), the slope of each line corresponds to $(1 - \beta)/\nu = 31/48$.

V. CONCLUSIONS

Jamming and percolation properties of linear bond k-mers on square lattices have been studied by numerical simulations and finite-size scaling analysis. Two models have been addressed: standard and inverse percolation.

In the case of standard percolation, linear bond k-mers (with k ranging between 1 and 120) were randomly and sequentially deposited on an initially empty lattice. In a first stage, the jamming properties were determined. A decreasing behavior was observed for the jamming coverage $p_{j,k}$, with a finite value of saturation in the limit of infinitely long k-mers: $p_{j,k} = A_j + B_j/k + C_j/k^2$ $(k \geqslant 1)$, $A_j = p_{j,k \to \infty} = 0.7476(1)$ being the jamming coverage for infinitely long bond k-mers, $B_j = 0.2165(5)$ and $C_j = 0.0360(5)$.

Once the limiting parameters $p_{j,k}$ were determined, the percolation properties of the system were studied. A monotonic decreasing dependence on k was found for the percolation threshold $p_{c,k}$, which decreases rapidly for small particles sizes (up to $k \approx 40$), and finally asymptotically converges toward a definite value for large segments. Following a similar scheme to that proposed for jamming properties, the curve of $p_{c,k}$ versus k was fitted as $p_{c,k} = A_c + B_c/k + C_c/k^2$ $(k \geqslant 5)$, $A_c = p_{c,k \to \infty} = 0.0033(9)$ being the limit percolation threshold by infinitely long bond k-mers, $B_c = 2.84(3)$ and $C_c = -5.7(2)$.

To conclude with the analysis of standard percolation, two points deserve to be highlighted: (1) the curve of $p_{j,k}$ remains above the curve of $p_{c,k}$, indicating that the percolation phase transition occurs for all values of k; and (2) the results obtained in the present paper represent a substantial improvement with

respect to previous work [31], where jamming and percolation properties of linear bond k-mers were studied for $1 \leqslant k \leqslant 40$ and small lattice sizes (values of L/k up to 56).

With respect to inverse percolation, the process starts with an initial configuration, where all lattice bonds are occupied and, obviously, the opposite sides of the lattice are connected by nearest-neighbor occupied bonds. Then, the system is diluted by randomly removing linear bond k-mers from the lattice. In this framework, the calculation of the inverse jamming coverage $p_{j,k}^i$ is trivial: $p_{j,k}^i = 1 - p_{j,k}$. Note that $p_{j,k}^i$ is the coverage of the limit state, in which no more objects can be removed from the lattice due to the absence of linear clusters of nearest-neighbor bonds of appropriate size.

On the other hand, the inverse percolation threshold $p_{c,k}^i$ is a decreasing function of k in the range $1 \leqslant k \leqslant 18$. For $k > 18$, all jammed configurations are percolating states, and consequently, there is no nonpercolating phase. The interplay between the percolation and the jamming effects is responsible for the existence of a maximum value of k (in this case, $k = 18$) from which the percolation phase transition no longer occurs. This behavior had not been observed previously. In fact, in the case of inverse percolation of linear site k-mers on square and triangular lattices, percolating and nonpercolating phases extend to infinity in the space of the parameter k [19,20].

It is interesting to analyze the results obtained for inverse percolation in terms of vulnerability and network attacks. In this context, the decreasing behavior of $p_{c,k}^i$ as a function of k clearly indicates that random attacks on single nodes ($k = 1$) are much more effective than correlated attacks on groups of close nodes. Moreover, for large k-mers ($k > 18$), the lattice remains connected even when the highest allowed concentration of removed bonds $p_{j,k}^i$ is reached. A similar behavior has been informed in recent papers [25,26], where the influence of the characteristics of the initial attack on the vulnerability of the networks has been studied. In this line, future studies will be carried out to investigate the effect of the structure of the attack (shape of the removed object) on the connectivity properties of the damaged lattice.

Finally, the accurate determination of critical exponents revealed that standard and inverse bond percolation models on square lattices belong to the same universality class as the random percolation, regardless of the size k considered.

[1] M. Sahimi, *Applications of Percolation Theory* (Taylor & Francis, London, 1992).

[2] D. Stauffer and A. Aharony, *Introduction to Percolation Theory* (Taylor & Francis, London, 1994).

[3] G. Grimmett, *Percolation* (Springer-Verlag, Berlin, 1999).

[4] B. Bollobás and O. Riordan, *Percolation* (Cambridge University Press, New York, 2006).

[5] J. Becklehimer and R. B. Pandey, Physica A (Amsterdam) **187**, 71 (1992).

[6] V. Cornette, A. J. Ramirez-Pastor, and F. Nieto, Physica A (Amsterdam) **327**, 71 (2003).

[7] V. Cornette, A. J. Ramirez-Pastor, and F. Nieto, Eur. Phys. J. B **36**, 391 (2003).

[8] Y. Leroyer and E. Pommiers, Phys. Rev. B **50**, 2795 (1994).

[9] B. Bonnier, M. Hontebeyrie, Y. Leroyer, C. Meyers, and E. Pommiers, Phys. Rev. E **49**, 305 (1994).

[10] N. Vandewalle, S. Galam, and M. Kramer, Eur. Phys. J. B **14**, 407 (2000).

[11] N. I. Lebovka, N. N. Karmazina, Y. Y. Tarasevich, and V. V. Laptev, Phys. Rev. E **84**, 061603 (2011).

[12] G. Kondrat and A. Pękalski, Phys. Rev. E **63**, 051108 (2001).

[13] Y. Y. Tarasevich, N. I. Lebovka, and V. V. Laptev, Phys. Rev. E **86**, 061116 (2012).

[14] Lj. Budinski-Petković, I. Lončarević, M. Petković, Z. M. Jakšić, and S. B. Vrhovac, Phys. Rev. E **85**, 061117 (2012).

[15] Lj. Budinski-Petković, I. Lončarević, Z. M. Jakšić, and S. B. Vrhovac, J. Stat. Mech. (2016) 053101.

[16] M. E. J. Newman, A.-L. Barabási, and D. J. Watts, *The Structure and Dynamics of Networks* (Princeton University Press, New Jersey, 2006).

[17] M. E. J. Newman, *Networks: An Introduction* (Oxford University Press, Oxford, UK, 2010).

[18] S. N. Dorogovtsev and J. F. F. Mendes, *Evolution of Networks: From Biological Nets to the Internet and WWW* (Oxford University Press, Oxford, UK, 2003).

[19] L. S. Ramirez, P. M. Centres, and A. J. Ramirez-Pastor, J. Stat. Mech. (2015) P09003.

[20] L. S. Ramirez, P. M. Centres, and A. J. Ramirez-Pastor, J. Stat. Mech. (2017) 113204.

[21] H. Hinrichsen, Adv. Phys. **49**, 815 (2000).

[22] P. L. Krapivsky, S. Redner, and E. Ben-Naim, *A Kinetic View of Statistical Physics* (Cambridge University Press, London, 2010).

[23] R. Albert, H. Jeong, and A.-L. Barabási, Nature **406**, 378 (2000).

[24] R. Albert and A.-L. Barabási, Rev. Mod. Phys. **74**, 47 (2002).

[25] Y. Kornbluth, S. Lowinger, G. A. Cwilich, and S. V. Buldyrev, Phys. Rev. E **89**, 032808 (2014).

[26] S. Lowinger, G. A. Cwilich, and S. V. Buldyrev, Phys. Rev. E **94**, 052306 (2016).

[27] J. W. Evans, Rev. Mod. Phys. **65**, 1281 (1993).

[28] G. D. García, F. O. Sanchez-Varretti, P. M. Centres, and A. J. Ramirez-Pastor, Physica A (Amsterdam) **436**, 558 (2015).

[29] P. M. Centres and A. J. Ramirez-Pastor, J. Stat. Mech. (2015) P10011.

[30] E. J. Perino, D. A. Matoz-Fernandez, P. M. Pasinetti, and A. J. Ramirez-Pastor, J. Stat. Mech. (2017) 073206.

[31] M. Dolz, F. Nieto, and A. J. Ramirez-Pastor, Phys. Rev. E **72**, 066129 (2005).

[32] F. Yonezawa, S. Sakamoto, and M. Hori, Phys. Rev. B **40**, 636 (1989).

[33] J. Hoshen and R. Kopelman, Phys. Rev. B **14**, 3438 (1976).

[34] S. Biswas, A. Kundu, and A. K. Chandra, Phys. Rev. E **83**, 021109 (2011).

[35] A. K. Chandra, Phys. Rev. E **85**, 021149 (2012).

[36] K. Binder, Rep. Prog. Phys. **60**, 487 (1997).

[37] M. E. J. Newman and R. M. Ziff, Phys. Rev. E **64**, 016706 (2001).

[38] R. M. Ziff and M. E. J. Newman, Phys. Rev. E **66**, 016129 (2002).